https://doi.org/10.20965/ijat.2018.p0688

Paper:

Milling Process Monitoring Based on Vibration Analysis Using Hilbert-Huang Transform

Agus Susanto*, Chia-Hung Liu, Keiji Yamada*,†, Yean-Ren Hwang***, Ryutaro Tanaka*, and Katsuhiko Sekiya***

*Graduate School of Engineering, Hiroshima University
1-4-1 Kagamiyama, Higashi-Hiroshima, Hiroshima 739-8527, Japan
†Corresponding author, E-mail: keiji@hiroshima-u.ac.jp
**Industrial Technology Research Institute, Hsinchu, Taiwan
***Department of Mechanical Engineering, National Central University, Taoyuan City, Taiwan
[Received April 2, 2018; accepted July 9, 2018]

Vibration analysis is one method of machining process monitoring. The vibration obtained in machining is often nonlinear and of a nonstationary nature. Therefore, an appropriate signal analysis is needed for signal processing and feature extraction. In this research, vibrations obtained in the milling of thin-walled workpieces were analyzed using the Hilbert-Huang transform (HHT). The features obtained by the HHT served as machining-state indicators for machining process monitoring. Experimental results showed the effectiveness of the HHT method for detecting chatter and tool damage.

Keywords: milling operation, vibration analysis, chatter, tool damage, Hilbert-Huang transform

1. Introduction

Thin-walled mechanical parts are extensively used in industries and academia [1, 2]. However, the machining of those parts is more challenging than that for rigid ones. The main reason for this is that the dynamic properties of the thin parts, such as stiffness and damping, are low. Besides, the machining of thin-walled parts can induce chatter vibration and tool wear, which affects the surface quality of the final product. Therefore, machining process monitoring is needed to make better products. An easy way for machining process monitoring is by analyzing vibration.

To suppress chatter vibration, the cutting parameters responsible for machining instability are often defined first. To this end, a stability lobe diagram (SLD) is generated prior to real machining. SLD in machining was first studied by Tobias et al. [3] and was extended by Tlusty [4] in high-speed milling, as well as by Altintas and Budak [5]. Furthermore, it has been widely applied in several research fields. Bravo et al. [6] used SLD for high-speed milling of monolithic workpieces. Campa et al. [7] proposed a methodology for chatter avoidance in the milling of flexible thin floors by using a bull-nose end mill by using a stability diagram. Alan et al. [8] generated an SLD for a multistage milling operation.

In analyzing vibration for machining process monitoring, an analysis in the frequency domain obtained by fast Fourier transform (FFT) is commonly used for chatter detection [9, 10]. However, time-frequency analysis (TFA) methods might be better suited, because machining states can be determined both in the time and frequency domains. A few researchers have used conventional TFA methods for machining process monitoring, such as short-time Fourier [11], Stockwell [12], and wavelet [13] transforms.

Vibration occurring in the machining process is often nonlinear and has a nonstationary nature [14]. Therefore, conventional signal analysis approaches are hampered when analyzing it. Instead, a nonlinear and nonstationary signal analysis method should be applied. The Hilbert-Huang transform (HHT) is one of the powerful TFA methods and deals with nonlinear and nonstationary signals [15–17].

The research presented here focused on end milling process monitoring of thin-walled workpieces by vibration analysis. The HHT was utilized to analyze the vibration obtained in milling tests to detect chatter and tool damage.

2. Dynamic Model in Milling and Signal Processing

2.1. Dynamic Model in Thin-Walled Milling

Because the rigidity in the thickness direction is especially low for thin walls, the dynamic model in milling of thin-walled structures can be simplified as forced vibration of a single-degree-of-freedom (SDOF) system, as shown in **Fig. 1**.

In this model, the thin-walled workpiece is considered a flexible part that is deformed by cutting forces. The model consists of modal mass m, stiffness k, and damping c to describe the vibrating displacement at the cutting

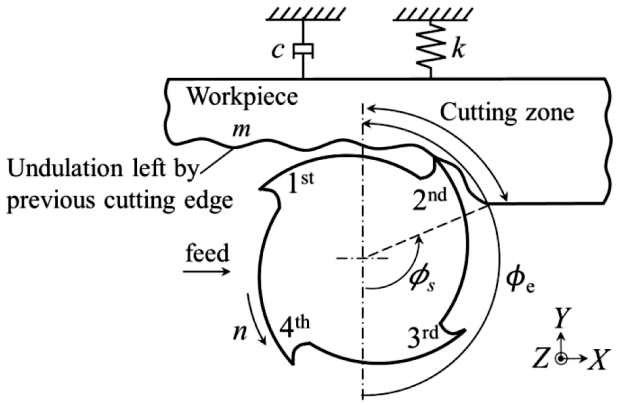

Fig. 1. Simplified dynamic model in thin-walled milling.

point caused by the workpiece deformation. A part of the workpiece surface is machined by a rotating tool. The depth of cut is constant when multiple teeth successively generate chips within a cutting zone whose length is given by $r_a(\phi_e - \phi_s)$. However, the effective cutting thickness fluctuates because of the vertical vibration of the workpiece. Cutting forces are also inconstant, and each tooth leaves an undulation behind, which affects the effective cutting thickness of the next tooth. Thus, this cycle continues as the vibrating displacement fluctuates with the force that excites the vibrating displacement itself.

The dynamic equation for SDOF forced vibration can be written as $m\ddot{y} + c\dot{y} + ky = f(t)$, with a harmonic force $f(t) = Fe^{i\omega t}$, where F is the vibration amplitude of force, i is the imaginary unit, ω is the force frequency, and t is time [18].

The steady-state solution for the equation is $y(t) = Ye^{i\omega t}$. Substituting this into the above equation, the result shows that the force is related to the resultant vibration of the force frequency ω as:

$$\left(-m\omega^2 + i\omega c + k\right) Ye^{i\omega t} = Fe^{i\omega t} \quad \ldots\ldots \quad (1)$$

Equation (1) can be rewritten as a ratio of the output to the input, which is well-known as the frequency response function (FRF):

$$G_{yy}(\omega) = \frac{Y}{F} = \frac{1}{k}\left[\left\{1 - \left(\frac{\omega}{\omega_n}\right)^2\right\} + i2\zeta\frac{\omega}{\omega_n}\right]^{-1} = \frac{1}{k}\frac{1}{(1-r^2) + i2\zeta r} \quad \ldots\ldots \quad (2)$$

where $\omega_n = \sqrt{k}/m$ is the natural frequency, $\zeta = (c/2m\omega_n)$ is the damping ratio, $r = (\omega/\omega_n)$ is the frequency ratio, and $G_{yy}(\omega)$ is the direct transfer function that represents the ratio between the output response in the y direction and the input excitation force in y. For convenience, converting the denominator to a real number yields:

$$G_{yy}(\omega) = \frac{1}{k}\frac{\left(1-r^2\right) - i2\zeta r}{\left(1-r^2\right)^2 + (2\zeta r)^2} \quad \ldots\ldots \quad (3)$$

Equation (3) shows a complex function that can be presented in real and imaginary parts in Eqs. (4)–(5) and magnitude and phase in Eqs. (6)–(7):

$$\mathrm{Re}\left\{G_{yy}(\omega)\right\} = \frac{1}{k}\frac{\left(1-r^2\right)}{\left(1-r^2\right)^2 + (2\zeta r)^2} \quad \ldots\ldots \quad (4)$$

$$\mathrm{Im}\left\{G_{yy}(\omega)\right\} = \frac{1}{k}\frac{-2\zeta r}{\left(1-r^2\right)^2 + (2\zeta r)^2} \quad \ldots\ldots \quad (5)$$

$$\left|G_{yy}(\omega)\right| = \frac{1}{k}\sqrt{\frac{1}{\left(1-r^2\right)^2 + (2\zeta r)^2}} \quad \ldots\ldots \quad (6)$$

$$\Psi = \tan^{-1}\left[\frac{\mathrm{Im}\left\{G_{yy}(\omega)\right\}}{\mathrm{Re}\left\{G_{yy}(\omega)\right\}}\right] \quad \ldots\ldots \quad (7)$$

According to Altintas and Budak [5], the FRF has a close relationship with the stability limit as follows:

$$\mathrm{Re}\left\{G_{yy}(\omega)\right\} = \frac{2\pi}{N_t K_t A_{alim}\alpha_{yy}} \quad \ldots\ldots \quad (8)$$

where N_t, K_t, and A_{alim} are the number of teeth, tangential milling force coefficient [N/m^2], and chatter-free axial cutting depth [mm], respectively. α_{yy} is the directional milling coefficient in the y-direction, which is obtained by integrating between start ϕ_s and exit ϕ_e angles when the cutting edge enters and exits the cutting zone given as [5]:

$$\alpha_{yy} = \frac{1}{2}\left[-\cos(2\phi) - 2K_r\phi - K_r\sin(2\phi)\right]_{\phi_s}^{\phi_e} \quad . \quad (9)$$

where K_r is the radial milling force coefficient [N/m^2]. In the model for down-milling operation, the exit angle ϕ_e is 180° and the start angle ϕ_s in degree is defined by the radial depth of cut A_r and the tool radius r_a as follows:

$$\phi_s = 180 - \cos^{-1}\left(\frac{r_a - A_r}{r_a}\right) \quad \ldots\ldots \quad (10)$$

When the self-excited vibration occurs, the frequency ω is defined by the spindle speed n [min^{-1}] and the phase ψ by Eq (7).

$$n = \frac{60\omega}{2l_b\pi + \Psi} \quad \ldots\ldots \quad (11)$$

where l_b is the integer number of lobes ($l_b = 0, 1, 2, \ldots$).

By iterative calculations of Eqs. (7)–(11) over a wide range of frequency ratios r for arbitrary integers l_b, the SLD can be obtained in which the stability limit of the axial cutting depth and the spindle speed are plotted together.

2.2. Fast Fourier Transform

Vibration analysis by FFT can provide the feature of vibration in a frequency spectrum, and it can be used to determine machining states. For the measured signal $x(t)$ with a sampling period T and the data length N, the FFT is given as [14]:

$$X(n) = \sum_{j=1}^{N} x(j)\, e^{-i2\pi(n-1)\frac{j-1}{j}} \quad \ldots\ldots \quad (12)$$

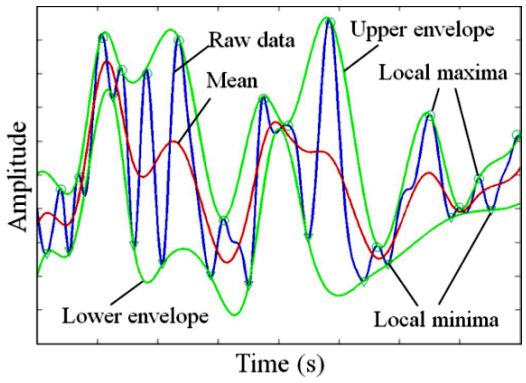

(a) Raw data, local minima and maxima, upper and lower envelopes, and mean of the envelopes.

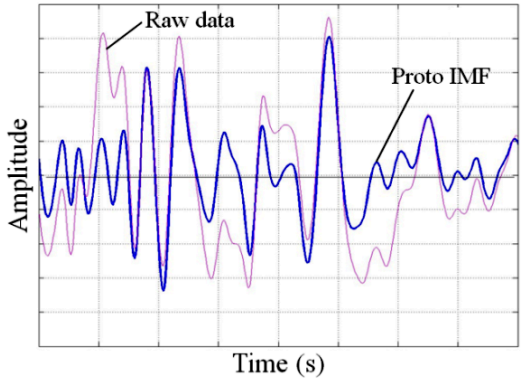

(b) Raw data and proto-IMF.

Fig. 2. Example of sifting process in EMD [15].

where $n = 1,2,\ldots,N$.

The frequency resolution Δf is defined as the ratio of sampling rate fs to the data length N, i.e., $\Delta f = fs/N$.

2.3. Hilbert-Huang Transform

The HHT method contains two consecutive steps. The first step is empirical mode decomposition (EMD), which decomposes a raw signal into a series of components called intrinsic mode functions (IMFs). The EMD process is summarized as follows [19]:

(1) **Figure 2(a)** shows the elementary process of EMD, in which the high-frequency component is sifted from given data $x(t)$. By interpolating all local maxima and minima of the data, the upper and the lower envelopes are found, the mean of which $m(t)$ is used to define a proto-IMF $h(t) = x(t) - m(t)$, as shown in **Fig. 2(b)**.

(2) Repeat (1) by replacing $h(t)$ with the given data $x(t)$ until the proto-IMF satisfies the stoppage criterion [15]. When the criterion is satisfied, IMF component is defined as $c(t) = h(t)$.

(3) The residue of data is $r(t) = x(t) - c(t)$, which replaces data $x(t)$ to repeat (1) and (2) until the residue $r(t)$ becomes a monotonic function. By repeating the above process for N_k times, IMF $= \{c_j(t)|j = 1,2,\ldots,N_k\}$ and a monotonic residue r_{Nk} are obtained. Finally, decomposition of the given $x(t)$ is achieved as:

$$x(t) = \sum_{j=1}^{Nk} \{c_j(t) + r_{Nk}(t)\} \quad . \quad . \quad . \quad . \quad . \quad . \quad (13)$$

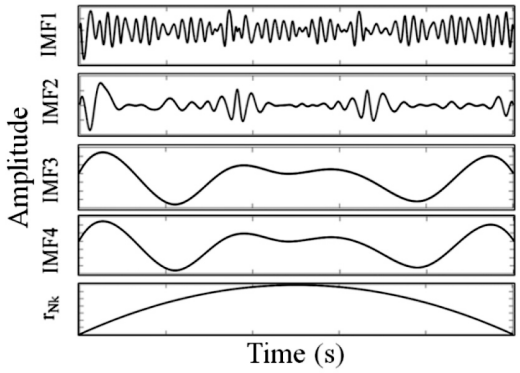

Fig. 3. Example of IMF components and monotonic residue obtained by EMD process [19].

Figure 3 shows an example of IMF components and the monotonic residue obtained by the EMD process for the acceleration signal measured in the milling operation [19].

The second step of the HHT is applying the Hilbert transform to all IMFs for generating an energy-time-frequency distribution that is called a Hilbert spectrum. The Hilbert transform for all IMFs can be expressed as [15]:

$$x(t) = \sum_{j=1}^{Nk} \left\{ a_j(t) \exp\left(i \int \omega(t)\, dt \right) \right\} \quad . \quad . \quad . \quad (14)$$

where $a_j(t)$ and $\omega(t)$ are the instantaneous amplitude and instantaneous frequency.

3. Experimental Procedures

3.1. Machine Tool, Workpiece, and End Mill

In milling tests, a three-axis knee-type computer-numerical-control milling machine was used, and workpieces were thin-walled plates with the dimensions 100 × 100 × 3 mm. The work material was 7055 aluminum alloy, which is widely used in studies [20] and industries [21]. The cutting tools used were HSS-Co square end mills, whose specifications are given in **Table 1**. In all milling tests, uncoated tools were used.

3.2. Dynamic Cutting System Identification

Before the milling tests, the modal parameters (m, c, and k) discussed in Section 2.1 had to be measured

Table 1. Specifications of end mill tool.

Terminology	Dimension
Diameter ϕ [mm]	12
Total length L [mm]	80
Helix angle b [°]	45
Number of teeth N_t	4

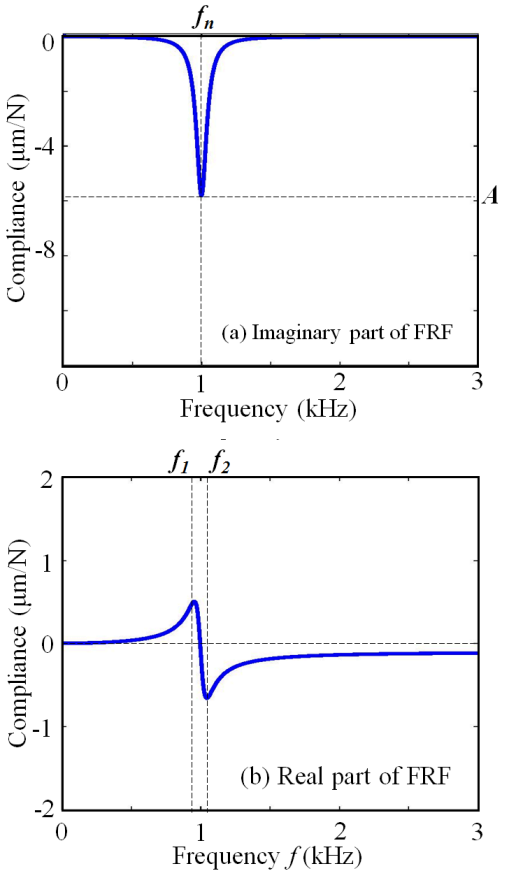

Fig. 4. FRFs of workpiece obtained by hammering tests.

through a hammering test to create an SLD. The constructed SLD was then used to determine the cutting parameters in all milling tests.

Figure 4 shows the FRFs for a workpiece obtained in the hammering test. **Fig. 4(a)** is the imaginary part of FRF that contains the natural frequency $f_n = 1$ kHz and negative peak value A. **Fig. 4(b)** is the real part of the FRF. It contains two frequencies f_1 and f_2 which correspond to the observed peaks. By using those values, f_n, A, f_1, and f_2, the modal parameters can be obtained by the experimental modal analysis technique [18], and the results are shown in **Table 2**.

Figure 5 shows the SLD generated based on the modal parameters, the down-milling process with a radial cutting depth $A_r = 0.5$ mm, and the use of the end-mill tool with a tooth number $N_t = 4$. Here, a tangential cutting-force coefficient $K_t = 7.96 \times 10^8$ N/m^2 and radial ones $K_r = 1.68 \times 10^8$ N/m^2 were also used by referring to

Table 2. Dynamic modal parameters of workpiece.

Vibration mode	Natural frequency f_n [kHz]	Damping ratio ζ [%]	Stiffness K [N/μm]
First	1	1.63	2.1

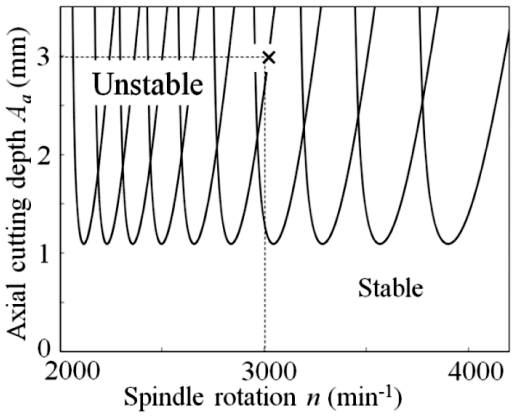

Fig. 5. Stability lobe diagram.

the work of Jin et al. [20]. This figure shows 10 lobes ($l_b = 0, 1, \ldots, 9$) generated for a spindle rotational speed of 2000–4500 min^{-1}. In the SLD, stable cutting occurs in the region below the lobes, while unstable cutting occurs above the lobes.

3.3. Milling Tests for Chatter Detection

The SLD in **Fig. 5** was used to select the cutting parameters: the axial cutting depth A_a and the spindle speed n. According to the diagram, $A_a = 3$ mm associated with $n = 3000$ min^{-1} were chosen as cutting parameters in milling tests under unstable conditions (see "×" symbol).

Figure 6 and **Table 3** show the experimental setup and cutting conditions, respectively. Side milling was performed with a tool overhang of 45 mm, and the vibration was measured by an accelerometer sensor and then stored by a digital storage scope – Yokogawa DL750.

3.4. Tests for Tool Monitoring

Three kinds of end-mill with different cutting-edge conditions were used, and the influence of the conditions was investigated. **Fig. 7** shows a microscopic photograph of the cutting edges.

Figure 7(a) is the end-mill body with four flutes in a normal condition. The cutting-edge magnification is shown in **Fig. 7(b)**. **Fig. 7(c)** shows the cutting edge for the worn tool that was simulated by grinding down on one of the teeth but retaining the cutting ability of the tooth. The condition of this worn tool was similar to flank wear. **Fig. 7(d)** shows a chipped tool. The chipped tool was simulated by grinding out the teeth completely, so that the ground tooth was unable to cut the workpiece.

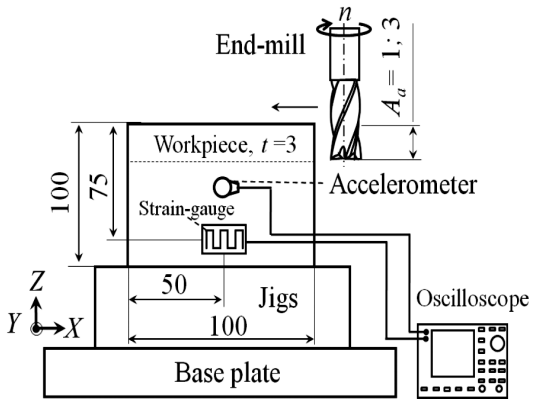

Fig. 6. Milling test setup and position of sensors.

Table 3. Cutting parameters for observing chatter.

Spindle rotation n [min^{-1}]	Cutting speed v_c [m/min]	Feed per tooth f_z [mm/tooth]	Depth of cut [mm]	
			Axial A_a	Radial A_r
3000	113	0.08	3	0.5

Milling tests were conducted in the stable area of the SLD. An axial cutting depth $A_a = 1$ mm corresponding to spindle rotation $n = 600$ min^{-1} was chosen as the cutting parameter. **Table 4** shows the cutting parameters in detail. The setup for the milling test is shown in **Fig. 6**. Cutting vibrations were measured by a strain gauge. The position of the strain gauge is also shown in this figure.

4. Results and Discussion

The obtained vibrations in milling of thin-walled workpieces were analyzed in the frequency domain by using the FFT and time-frequency domain using the HHT. The results are discussed in the following section.

4.1. Chatter Identification

Figure 8 shows a full vibration signal that was measured in milling under stable cutting conditions, given in **Table 3**. This figure contains the data length N of 700,000 points, and the sampling rate was at 100 kHz.

As shown in the figure, the acceleration signal shows varying amplitudes over the cutting period. The amplitude increases from the start of machining until 2.5 s (see the box for region a). That amplitude stabilizes at a cutting period of 3.3–4.5 s (see the box for region b) and increases again from 4.6 s until finish (see the box for region c). The occurrence of chatter is shown in the increase of vibrational amplitude. Conversely, the decrease in vibrational amplitude indicates the absence of chatter. The vibrational pattern in **Fig. 8** also appeared in the texture of the finished surface, as shown in **Fig. 9**. Here, the machined surface was also divided into three regions that correspond to the vibration shown in **Fig. 8**.

The frequency contents were observed through acceleration signal analysis in the solid boxes of **Fig. 8**. The magnified boxes are displayed in **Fig. 10**. The transient acceleration signals containing chatter are shown in **Figs. 10(a)** and **(c)**. However, the transient acceleration signal containing no chatter is shown in **Fig. 10(b)**. Furthermore, the frequency content of these vibrations was observed using the FFT in the next section.

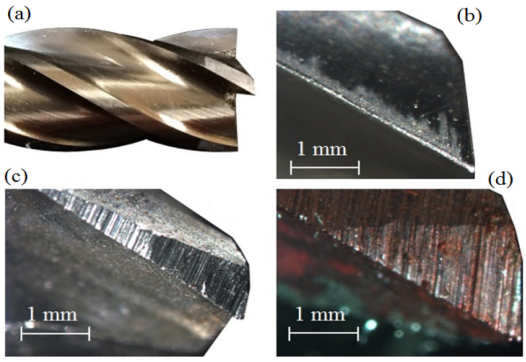

Fig. 7. Microscopic photograph of different cutting edges: (a) full end-mill body, (b) normal, (c) worn, and (d) chipped.

Table 4. Cutting parameters to observe tool conditions.

Spindle rotation n [min^{-1}]	Cutting speed v_c [m/min]	Feed per tooth f_z [mm/tooth]	Depth of cut [mm]		Tool condition
			Axial A_a	Radial A_r	
600	23	0.05	1	0.5	Normal
600	23	0.05	1	0.5	Wear
600	23	0.05	1	0.5	Chipping

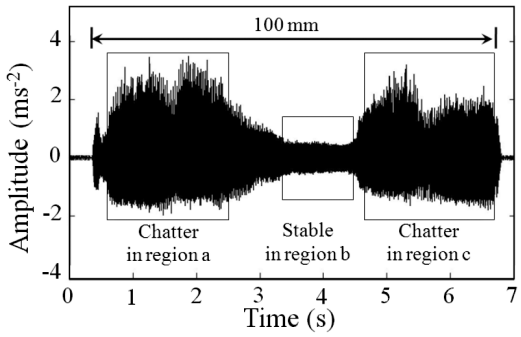

Fig. 8. Transient acceleration signal obtained in milling test.

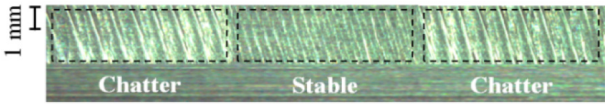

Fig. 9. Surface finish obtained in milling test.

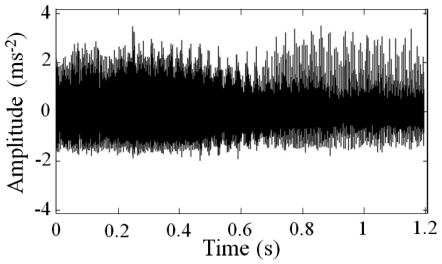

(a) Vibration for region a

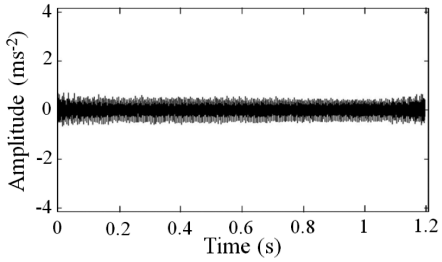

(b) Vibration for region b

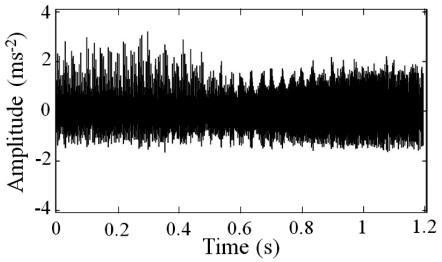

(c) Vibration for region c

Fig. 10. Magnified acceleration signals corresponding to **Fig. 8**.

4.1.1. Vibrations Analysis Using FFT

All vibrations in **Fig. 10** were analyzed by using the FFT, which was used to observe whether chatter frequency occurs. The waterfall of the frequency spectrum obtained by FFT is shown in **Fig. 11**. The time interval of 1.2 s was used to obtain this frequency spectrum.

According to **Fig. 11**, several frequencies appear in the frequency band. In this figure, the frequency of spindle rotation ($f_{sp} = n/60 = 50$ Hz), chatter (f_c), tooth passing ($f_p = N_t f_{sp} = 200$ Hz), and its harmonics (arrows symbol) are displayed in this figure.

Vibration in the machining process can be forced vibration and self-excited vibration (chatter). Forced vibration in machining occurs when the frequency components of vibration only exist at multiples of spindle rotational frequency, and another frequency is chatter. Therefore, the chatter phenomenon appears most prominently in regions a and c.

Figure 11 (region a) shows that chatter frequency appears at 2.74 kHz with the largest amplitude. This chatter frequency vanishes when the cutting process enters region b. Based on **Fig. 11** (region b), only the harmonics of the tooth-passing frequency appear in the frequency spectrum. During stable cutting, the vibration mainly focused on the spindle rotation, tooth passing, and harmonics frequencies. However, the chatter frequency reappears when the cutting process enters region c with the same chatter frequency.

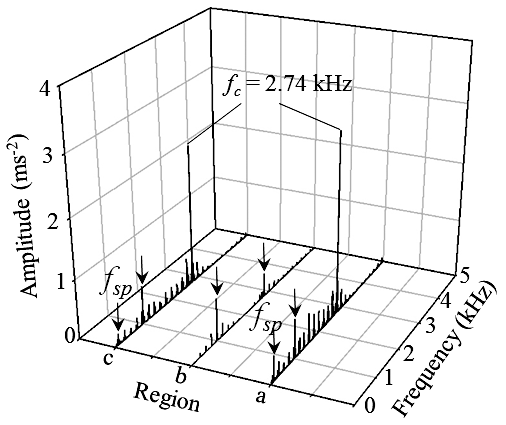

Fig. 11. Frequency spectrum obtained by FFT.

4.1.2. Vibration Analysis Using HHT

The EMD process was used to decompose the raw signal to be a series of IMF components, as shown in **Fig. 12**. Nine IMFs and a monotonic residue were obtained for regions a, b, and c. However, the fifth IMF c_5 to ninth IMF c_9 showed only the harmonics of the tooth-passing frequency. Therefore, the first four IMFs (c_1 to c_4) are shown for all milling case conditions. The harmonics of the tooth-passing frequency is a forced vibration in machining that occurs at multiples of spindle frequency, so it was not considered a significant vibration. They could be ignored and the monotonic-residue as well.

Figure 12 shows that each IMF component contains different oscillations and amplitudes. For example, first IMF c_1 contains the most oscillation. Otherwise, last IMF c_4 contains the least oscillation. Therefore, c_1 contains the highest frequency and c_4 contains the lowest frequency among all IMFs.

The fourth IMF c_4 in **Fig. 12(b)** and the second IMF c_2 in **Figs. 12(a)** and **(c)** capture the highest amplitude among IMF components for each region in the milling test. Therefore, each IMF contains unique information of the vibration mode.

To confirm the above deduction, all IMFs in **Fig. 12** were examined by using the FFT to observe the frequency content of each IMF, and the results are shown in **Fig. 13**. The time interval of 1.2 s was used to obtain these frequency spectra. All the symbols in these figures have the same denotations as in **Fig. 11**.

Every characteristic frequency appears in each IMF of **Fig. 13** with different amplitudes. Each IMF component contains one unique frequency, which means that the sifting process by EMD separated the complex vibration into simple components. For example, the first IMF c_1 includes the harmonic of the tooth-passing frequency with a certain amplitude for milling in all regions. In **Figs. 13(a)** and **(c)**, the second IMF c_2 includes the chatter frequency

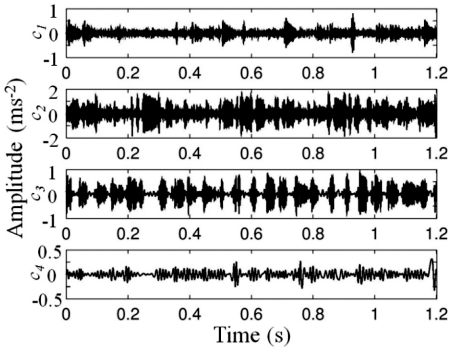

(a) IMFs for region a (unstable)

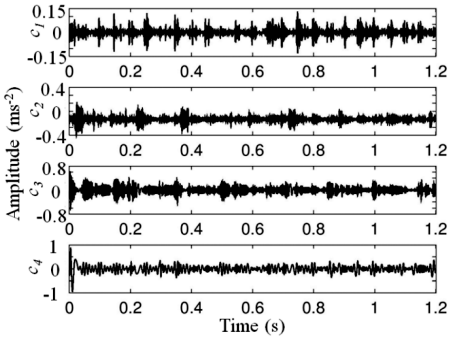

(b) IMFs for region b (stable)

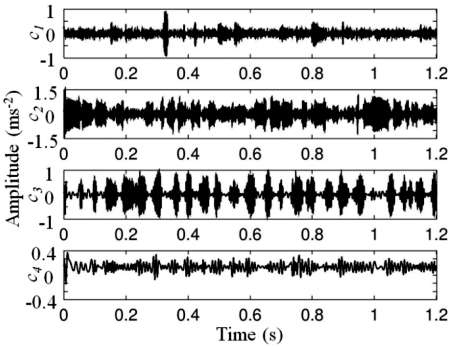

(c) IMFs for region c (unstable)

Fig. 12. IMFs in time domain obtained by EMD process for vibration produced in milling.

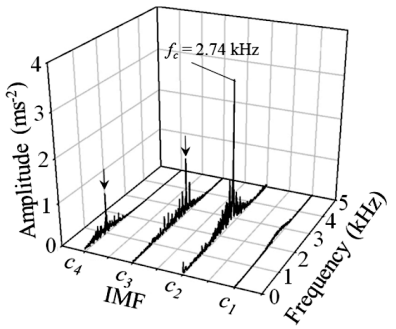

(a) IMFs for region a (unstable)

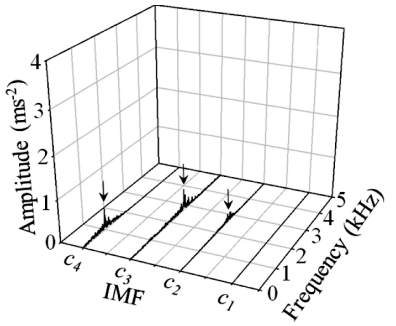

(b) IMFs for region b (stable)

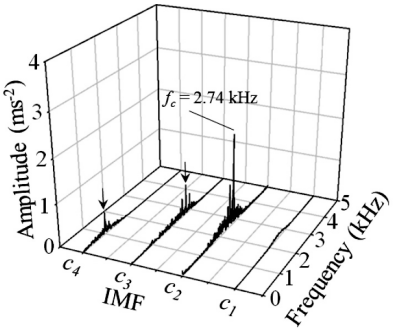

(c) IMFs for region c (unstable)

Fig. 13. Frequency spectra for each IMF obtained by FFT.

(2.74 kHz); c_3 and c_4 in **Fig. 13** show the harmonic of the tooth-passing frequency.

The above results show that the EMD process separated complex vibration into simple components, and each one of them contained a unique vibration mode caused by machining. EMD also sifted out the chatter from the others. In this study, the second IMF c_2 in **Figs. 13(a)** and **(c)** was a chatter-containing signal, whereas the other IMFs were signals without chatter. Thus, IMFs obtained by the EMD process made it easy for chatter identification.

Next, chatter was detected in the energy-time-frequency distribution, which is represented in the Hilbert spectrum shown in **Fig. 14**. According to these figures, milling states can be monitored in the time and frequency domains for all regions.

Figures 14(a) and **(c)** are Hilbert spectra for unstable milling, whereas **Fig. 14(b)** is for stable milling. Visual investigation of **Fig. 14** shows that the energy level for unstable milling was greater and fluctuated. The energy appearing in an unstable frequency could be caused by chatter. However, in **Fig. 14(b)**, the energy is concentrated in the natural frequency (1 kHz) over the cutting period.

4.2. Tool Damage Detection

Figure 15 shows strain signals measured in milling under the cutting conditions given in Section 3.4. **Fig. 15(a)** is a strain signal for the normal cutting edge of the end mill. The shapes of the peak mostly have the same forms and smaller amplitude than others. This figure shows that the period for one spindle rotation is approximately 0.1 s. It is associated with spindle rotation $n = 600$ min^{-1}. There are four peaks within one spindle rotation, and one peak of the signal was performed by one individual cutting edge of the end mill.

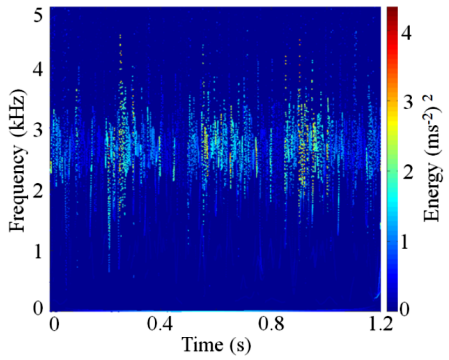

(a) Hilbert spectra for region (a) (unstable milling)

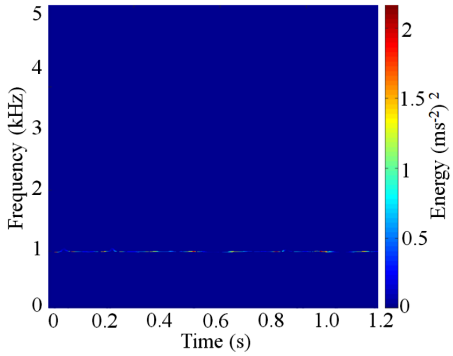

(b) Hilbert spectra for region (b) (stable milling)

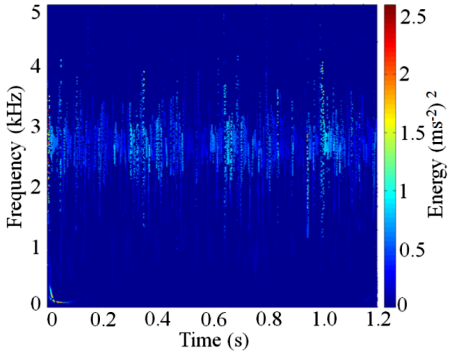

(c) Hilbert spectra for region (c) (unstable milling)

Fig. 14. Hilbert spectra for milling states monitoring.

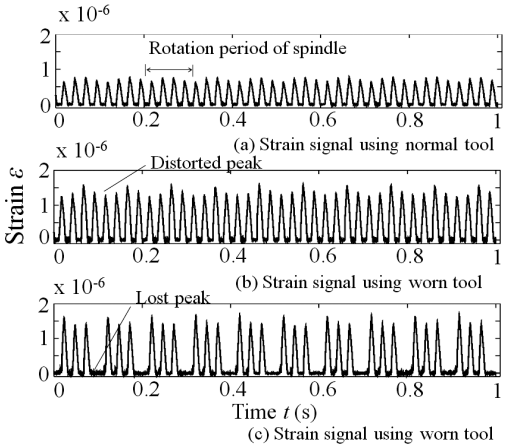

Fig. 15. Strain signals measured in milling using different tool conditions: (a) normal, (b) wear, and (c) chipping.

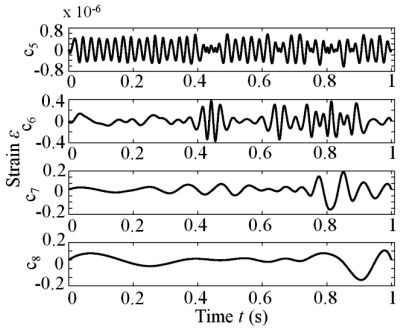

(a) IMFs associated to normal tool

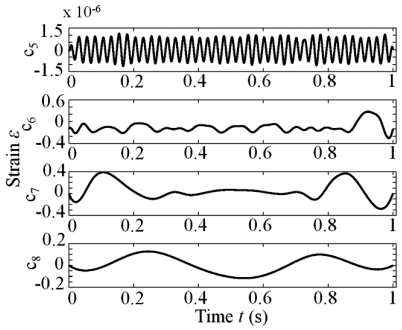

(b) IMFs associated to worn tool

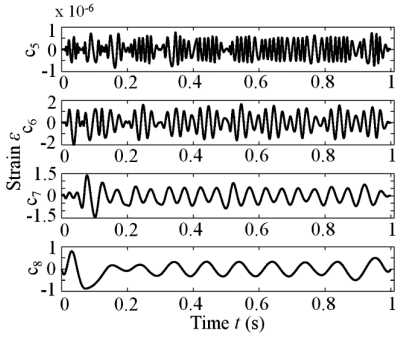

(c) IMFs associated to chipped tool

Fig. 16. IMF components obtained by EMD process associated with different tool conditions.

Figure 15(b) shows the strain signal measured in milling using the worn cutting edge of the end mill. According to this figure, one of the signal peaks is distorted within one spindle rotation. The distorted signal was caused by tool wear. **Fig. 15(c)** is the strain signal for the chipped end mill. One of the signal peaks is lost within one spindle rotation. The loss of the signal peak was caused by the tool having lost one of the cutting edges. As a result, only three signal peaks appeared within one spindle rotation.

4.2.1. Tool Damage Detection by HHT

Figure 16 shows IMF components obtained by the EMD process. Twelve IMFs and a monotonic residue resulted from this process. However, just four IMFs (c_5 to c_8) were shown for each milling condition, because these IMFs contained vibration modes that needed to be observed.

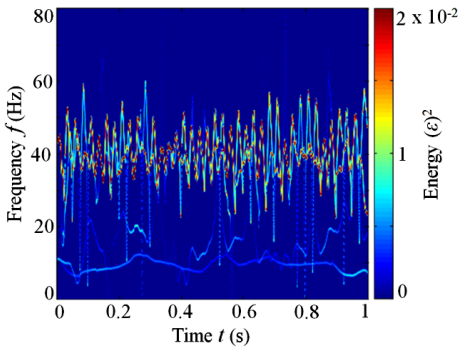

(a) Hilbert spectra associated with normal tool

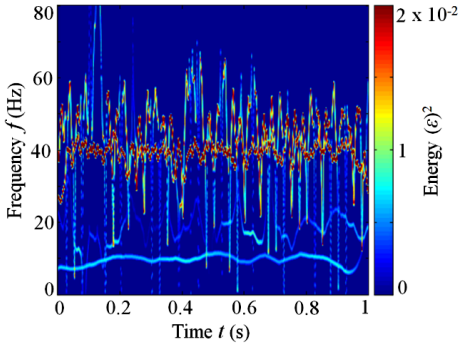

(b) Hilbert spectra associated with worn tool

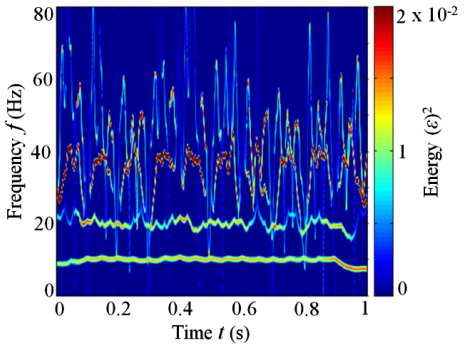

(c) Hilbert spectra associated with chipped tool

Fig. 17. Hilbert spectra for monitoring tool condition in milling.

Figures 16(a), **(b)**, and **(c)** are IMFs associated with milling using normal, worn, and chipped tools, respectively. The figures show an obvious change of the amplitudes in each IMF. The IMFs associated with milling using a normal tool contain smaller amplitudes than those using worn or chipped tools.

The intrinsic meaning of each IMF was explored in time-frequency domain using the Hilbert transform for tool condition monitoring, and the result is displayed in the Hilbert spectrum. In this study, the energy only appeared at low frequency. Therefore, the frequency band was narrowed to 0–80 Hz to analyze vibrations in more detail, as shown in **Fig. 17**. Based on **Fig. 17**, tool conditions can be monitored based on the energy distribution in the time-frequency domain.

Figure 17(a) shows the Hilbert spectrum associated with the strain signal measured in milling using the normal tool. As can be seen from the figure, the energy appears at the frequency of 40 Hz over the cutting period. This is the tooth-passing frequency ($f_p = N_t f_s = 40$ Hz). **Fig. 17(b)** shows the Hilbert spectrum associated with milling using the worn tool. In this figure, the energy appears in the tooth-passing frequency of 40 Hz and spindle rotation frequency ($f_s = n/60 = 10$ Hz). However, **Fig. 17(c)** shows the Hilbert spectrum associated with milling using a chipped tool. According to this figure, the energy appears in three frequency components: 10, 25, and 40 Hz.

As the above results show, tool conditions can be monitored as follow. When the end mill began to wear, the energy in the Hilbert spectrum appeared at spindle rotation frequency, whereas, when the end mill was chipping, the energy appeared in the spindle rotation, tooth passing, and new frequencies.

5. Conclusions

This study focused on milling process monitoring through analyzing vibrations and utilized the HHT and FFT for analyzing vibrations. Here are some important conclusions.

1. Chatter occurred in some specific zones of a thin-walled workpiece during milling. For identifying the chatter vibration, the EMD was more useful compared with the FFT method. The EMD could sift out the signal containing chatter from the signal containing spindle rotation, tooth passing, and its harmonic frequencies.

2. The HHT provided useful features for milling process monitoring, unlike the FFT. Both chatter and tool condition can be monitored by the Hilbert spectrum in the time and frequency domains. Moreover, worn and chipped tools can be distinguished from normal tools by the Hilbert spectrum.

3. In this study, the strain signal provided a useful signal for tool condition monitoring with the HHT.

References:

[1] M. A. Butt, Y. Yang, X. Pei, and Q. Liu, "Five-axis milling vibration attenuation of freeform thin-walled part by eddy current damping," Precision Engineering, Vol.51, pp. 682-690, 2018.
[2] K. Kolluru and D. Axinte, "Coupled interaction of dynamic responses of tool and workpiece in thin wall milling," J. of Materials Processing Technology, Vol.213, No.9, pp. 1565-1574, 2013.
[3] S. A. Tobias and W. Fishwick, "Theory of regenerative machine tool chatter," Engineer, Vol.205, pp. 199-203, 1958.
[4] J. Tlusty, "Dynamics of high-speed milling," J. of Engineering Industry for Trans. of ASME, Vol.108, pp. 59-67, 1986.
[5] Y. Altintas and E. Budak, "Analytical prediction of stability lobes in milling," CIRP Annals, Vol.44, No.1, pp. 357-362, 1995.
[6] U. Bravo, O. Altuzarra, L. N. L. Lacalle, J. A. Sánchez, and F. J. Campa, "Stability limits of milling considering the flexibility of the workpiece and the machine," Int. J. of Machine Tools and Manufacture, Vol.45, No.15, pp. 1669-1680, 2005.
[7] F. J. Campa, L. N. L. Lacalle, and A. Celaya, "Chatter avoidance in the milling of thin floors with bull-nose end mills: Model and stability diagrams," Int. J. of Machine Tools and Manufacture, Vol.51, No.1, pp. 43-53, 2011.

[8] S. Alan, E. Budak, and H. N. Özgüven, "Analytical prediction of part dynamics for machining stability analysis," Int. J. Automation Technol., Vol.4. No.3, pp. 259-267, 2010.
[9] P. L. Huang, J. F. Li, J. Sun, and J. Zhou, "Study on performance in dry milling aeronautical titanium alloy thin-wall components with two types of tools," J. of Cleaner Production, Vol.67, pp. 258-264, 2014.
[10] K. Shimana, E. Kondo, H. Karashima, and N. Kawagoishi, "Fast detection of chatter in end-milling using pseudo auto-correlation function," Int. J. Automation Technol., Vol.6, No.6, pp. 728-735, 2012.
[11] Y. Yamada, T. Kadota, S. Sakata, J. Tachibana, K. Nakanishi, M. Sawada, and Y. Kakinuma, "Integrated chatter monitoring based on sensorless cutting force/torque estimation in parallel turning," Int. J. Automation Technol., Vol.11, No.2, pp. 215-225, 2017.
[12] I. N. Tansel, X. Wang, P. Chen, A. Yenilmez, and B. Ozcelik, "Transformations in machining. Part 2. Evaluation of machining quality and detection of chatter in turning by using S-transformation," Int. J. of Machine Tools and Manufacture, Vol.46, No.1, pp. 43-50, 2006.
[13] J. Xu, K. Yamada, K. Sekiya, R. Tanaka, and Y. Yamane, "Effect of different features to drill-wear prediction with back propagation neural network," Precision Engineering, Vol.38, No.4, pp. 791-798, 2014.
[14] A. Y. C. Nee (Ed.), "Handbook of Manufacturing Engineering and Technology," Springer, 2014.
[15] N. E. Huang and S. P. Shen (Eds.), "Hilbert-Huang Transform and Its Applications," World Scientific, 2005.
[16] S. Kato and M. Larson, "Time-frequency analysis of turbidity using the Hilbert-Huang transform," Proc. of Coastal Engineering, Vol.55, pp. 621-625, 2008 (in Japanese).
[17] J. Otsuka, "Unsteady nonlinear signal analysis using Hilbert-Huang transform," Monthly report of the civil engineering Research institute for cold region. No. 703, pp. 39-44, 2011 (in Japanese).
[18] T. L. Schmitz and K. S. Smith, "Mechanical Vibrations: Modeling and Measurement," Springer, 2012.
[19] A. Susanto, K. Yamada, K. Mani, R. Tanaka, and K. Sekiya, "Vibration Analysis in Milling of Thin-Walled Workpieces using Hilbert-Huang Transform," Proc. 9th Int. Conf. on Leading Edge Manufacturing in the 21st Century, Hiroshima, Japan, 2017.
[20] X. Jin, Y. Sun, Q. Guo, and D. Guo, "3D stability lobe considering the helix angle effect in thin-wall milling," I. J. Adv. Manufacturing and Tech., Vol.82, No.9-12, pp. 2123-2136, 2016.
[21] E. A. Starke Jr and J. T. Staley, "Application of modern aluminum alloys to aircraft," Progress in Aerospace Sciences, Vol.32, No.2-3, pp. 131-172, 1996.

Name:
Agus Susanto

Affiliation:
Doctoral Student, Graduate School of Engineering, Hiroshima University

Address:
1-4-1 Kagamiyama, Higashi-Hiroshima, Hiroshima 739-8527, Japan

Brief Biographical History:
2011- Master Student in Mechanical Engineering, Sepuluh Nopember Institute of Technology

Main Works:
• "Vibration Analysis in Milling of Thin-Walled Workpieces using Hilbert-Huang Transform," 9th Int. Conf. on Leading Edge Manufacturing in the 21st Century, Hiroshima, Japan, 2017.
• "Application of Hilbert-Huang transform for vibration signal analysis in end-milling," Precision Engineering, Vol.53, 2018.

Membership in Academic Societies:
• Japan Society for Precision Engineering (JSPE)

Name:
Chia-Hung Liu

Affiliation:
Deputy Engineer, Industrial Technology Research Institute (ITRI)

Address:
195 Sec. 4, Chung Hsing Rd., Chutung, Hsinchu 31057, Taiwan

Brief Biographical History:
2015- Master Student in Opto-Mechatronics Engineering, National Central University
2015- Master Student in Mechanical Systems Engineering, Hiroshima University
2017- Deputy Engineer, Industrial Technology Research Institute (ITRI)

Main Works:
• "Hilbert-Huang transform applied on vibration analyzing in end-milling process," JSPE Autum Conf., Japan, 2015.

Membership in Academic Societies:
• Japan Society for Precision Engineering (JSPE)
• Chinese Society of Mechanical Engineers (CSME)

Name:
Keiji Yamada

Affiliation:
Professor, Graduate School of Engineering, Hiroshima University

Address:
1-4-1 Kagamiyama, Higashi-hiroshima, Hiroshima 739-8527, Japan

Brief Biographical History:
1992- Research Associate, Kanazawa University
2002- Lecturer, Kanazawa University
2005- Associate Professor, Hiroshima University
2015- Professor, Hiroshima University

Main Works:
• "Thermal Stress Cleaving of Brittle Materials by Laser Beam," CIRP Annals, Vol.51, No.1, pp. 149-152, 2002.
• "Evaluation of Adhesion on Tool-Chip Interface with Dynamic Components of Cutting Force," J. of the JSPE, Vol.76, No.8, pp. 926-932, 2010.
• "A Study on Aspects of Attrition Wear of Cutting Grains in Grinding Process," Int. J. of Precision Engineering and Manufacturing, Vol.12, No.6, pp. 965-973, 2011.

Membership in Academic Societies:
• Japan Society for Precision Engineering (JSPE)
• Japan Society of Mechanical Engineers (JSME)
• Japan Laser Processing Society (JLPS)
• Japan Society for Abrasive Technology (JSAT)

Name:
Yean-Ren Hwang

Affiliation:
Professor, Department of Mechanical Engineering, National Central University

Address:
No. 300, Zhongda Rd., Zhongli District, Taoyuan City 32001, Taiwan

Brief Biographical History:
1994- Associate Professor, National Central University
2002- Professor, National Central University

Main Works:
• "A cutter tool monitoring in machining process using Hilbert-Huang transform," Int. J. of Machine Tools and Manufacture, Vol.50, No.5, pp. 495-501, 2010.
• "Impact of various ball cutter tool positions on the surface integrity of low carbon steel," Materials and Design, Vol.30, No.9, pp. 3360-3366, 2009.
• "Five-Axis Tool Orientation Smoothing Using Quaternion Interpolation Algorithm," Int. J. of Machine Tools and Manufacture, Vol.43, No.12, pp. 1259-1267, 2003.

Membership in Academic Societies:
• Taiwan Society of Electrical Machining Engineers (TSEME)
• China Society for Mechanical Engineering (CSME)

Name:
Ryutaro Tanaka

Affiliation:
Associate Professor, Graduate School of Engineering, Hiroshima University

Address:
1-4-1 Kagamiyama, Higashi-hiroshima, Hiroshima 739-8527, Japan

Brief Biographical History:
2003- Research Associate, Kanazawa University
2009- Lecturer, Kanazawa University
2012- Associate Professor, Hiroshima University

Main Works:
• "Development of tool edge temperature measurement method in wet cutting: Application for CBN and poly crystalline diamond tools," J. of Advanced Mechanical Design, Systems, and Manufacturing, Vol.6, No.6, pp. 916-922, 2012.
• "Influence of cutting fluid on tool edge temperature in end milling titanium alloy," J. of Advanced Mechanical Design, Systems, and Manufacturing, Vol.9, No.5, p. JAMDSM0074, 2015.
• "A new quantitative evaluation for characteristic of surface roughness in turning," Precision Engineering, Vol.50, pp. 20-26, 2017.

Membership in Academic Societies:
• Japan Society for Precision Engineering (JSPE)
• Japan Society of Mechanical Engineers (JSME)
• Japan Society for Abrasive Technology (JSAT)

Name:
Katsuhiko Sekiya

Affiliation:
Assistant Professor, Graduate School of Engineering, Hiroshima University

Address:
1-4-1 Kagamiyama, Higashi-hiroshima, Hiroshima 739-8527, Japan

Brief Biographical History:
1998- Hiroshima University

Main Works:
• "Tool wear under high-speed end-milling of Nickel-based superalloy Inconel 718," J. of the JSPE, Contributed papers, Vol.70, No.8, pp. 1086-1090, 2004.
• "Evaluation of Adhesion on Tool-Chip Interface with Dynamic Components of Cutting Force," J. of the JSPE, Vol.76, No.8, pp. 926-932, 2010.

Membership in Academic Societies:
• Japan Society for Precision Engineering (JSPS)
• Japan Society of Mechanical Engineers (JSME)
• Japan Society for Abrasive Technology (JSAT)